# Solitary Waves in a Discrete Nonlinear Dirac equation

Jesús Cuevas–Maraver
*Grupo de Física No Lineal, Departamento de Física Aplicada I,*
*Universidad de Sevilla. Escuela Politécnica Superior, C/ Virgen de África, 7, 41011-Sevilla, Spain*
*Instituto de Matemáticas de la Universidad de Sevilla (IMUS). Edificio Celestino Mutis. Avda. Reina Mercedes s/n, 41012-Sevilla, Spain*

Panayotis G. Kevrekidis
*Department of Mathematics and Statistics, University of Massachusetts, Amherst, MA 01003-9305, USA*

Avadh Saxena
*Center for Nonlinear Studies and Theoretical Division,*
*Los Alamos National Laboratory, Los Alamos, New Mexico 87545, USA*

In the present work, we introduce a discrete formulation of the nonlinear Dirac equation in the form of a discretization of the Gross-Neveu model. The motivation for this discrete model proposal is both computational (near the continuum limit) and theoretical (using the understanding of the anti-continuum limit of vanishing coupling). Numerous unexpected features are identified including a staggered solitary pattern emerging from a single site excitation, as well as two- and three-site excitations playing a role analogous to one- and two-site, respectively, excitations of the discrete nonlinear Schrödinger analogue of the model. Stability exchanges between the two- and three-site states are identified, as well as instabilities that appear to be persistent over the coupling strength $\epsilon$, for a subcritical value of the propagation constant $\Lambda$. Variations of the propagation constant, coupling parameter and nonlinearity exponent are all examined in terms of their existence and stability implications and long dynamical simulations are used to unravel the evolutionary phenomenology of the system (when unstable).

## I. INTRODUCTION

Nonlinear dispersive waves in physical systems are often described by the nonlinear Schrödinger equation (NLSE), which is both mathematically and physically studied in a broad range of settings including atomic physics [1], nonlinear optics [2] and mathematical physics [3, 4]. Both the continuum and the discrete [5, 6] installment of the equation have been analyzed in detail. A principal focus of the relevant properties, aside from issues of self-focusing and wave collapse [3] has been the study of the existence, stability and dynamics of solitary waves in this model, both in lower-dimensional settings (such as one-dimensional solitons and multi-solitons) and in higher dimensional settings (vortices, vortex rings, and related structures).

However, recent years have seen a gradual increase of interest in the study of near-relativistic settings, where a suitable generalization/extension of the NLSE is the so-called nonlinear Dirac equation (NLDE) [7]. In fact, a modified form of the NLSE (with additional terms) is a special case limit of the NLDE at the low-energy limit as has been demonstrated in [8]. Different realizations of the NLDE have been proposed in the realm of high energy physics, including the so-called massive Gross-Neveu model [9], as well as the massive Thirring model [10]. Importantly, the equation has seen a significant volume of studies from a more mathematical perspective. Various aspects have been examined in this context, including the spectral stability and the potential emergence of point spectrum eigenvalues with nonzero real part (which has been shown to be impossible to happen beyond the so-called embedded thresholds) [11], the orbital and asymptotic stability under a series of relevant assumptions [12]; see also the relevant works of [13–15], the nonlinear Schrödinger (non-relativistic) limit and its instability for nonlinearities beyond a critical exponent [16], as well as classical (Vakhitov-Kolokolov) and more suitable to this setting (energy based) criteria [17] for the linear stability of solitary waves in the NLDE. A series of more computationally/physically oriented studies both in the context of the stability/dynamics of the NLDE solitary waves [18, 19] (again, in principle for arbitrary nonlinearity powers) and in that of these structures in the presence of external fields [20] have also recently appeared.

It would be relevant to mention, at least in passing, one more framework where Dirac-type equations have received significant attention in recent years in the context of atomic Bose-Einstein condensates. This is, in particular, in the context of artificial gauge fields more broadly, and more specifically spin-orbit coupled Bose-Einstein condensates [21]. There, admittedly, the setup is somewhat different, as both the Dirac type operator and the Schrödinger one co-exist, but it is relevant to point out that such settings have already been realized experimentally [22–26]. Moreover, a wide range of coherent structures has been already proposed in them including vortices [27, 28], Skyrmions [29], Dirac monopoles [30] and dark solitons [31, 32], as well as self-trapped states [33], bright solitons [34, 35] and gap-solitons [36]. It has also been demonstrated that in such systems it is possible to create stable vortex solitons in free space, which until recently was considered impossible due to the presence of collapse, driven by the self-attractive cubic nonlinearity [37]. Finally, it is worthwhile to note in passing that a different setup where a discrete version of a model based on first-order PDEs was examined was that of a Bragg-grating system in [38].

In the present work, we will take a somewhat different path from the above works. In particular, we will consider a relatively

standard example of the NLDE (namely the so-called massive Gross-Neveu model), but motivated by the significant level of understanding and analytical tractability afforded by discrete settings [5, 6], we will instead consider a *spatially discrete form* of the NLDE. A significant part of our motivation for this consideration (and for the particular form of the selected discretization) is due to (a) the possibility to deploy the technology of the so-called anti-continuum (AC) limit of MacKay-Aubry [39], in order to appreciate the stability properties near the limit of uncoupled adjacent sites and (b) the feature that in the continuum limit of, in principle, infinite coupling, our conclusions are expected to connect to what is known for the corresponding PDE models that have been explored in the literature. Admittedly, the discretization that is selected herein is, arguably, not the most natural possible one (in that we utilize next-nearest neighbors in order to discretize the first derivative terms by centered differences). Nevertheless, it is identified that it is the most suitable one for the present setting type of stencil and discrete solitary waves are systematically obtained from the AC limit. Moreover, a very recent development worth noting is that spin-orbit Bose-Einstein condensates have recently been considered in the realm of an optical lattice [40], which is often thought (in the so-called superfluid regime) as being tantamount to a discretization of the original continuum problem, through a suitable Wannier function reduction [41]. This suggests that considering discrete variants of Dirac models may be a natural step for near future considerations.

While many of our findings are somewhat reminiscent of the corresponding discrete nonlinear Schrödinger (DNLS) equation ones [5, 6], numerous others are rather unique to the Dirac equation. The single site solution is found to lead to a rather unexpected waveform. The envelope of the latter will be seen to approach in the continuum limit to the solution of a different homoclinic state problem that will be explicitly discussed below. On the other hand, it is the two-site and three-site solutions that lead to a continuation all the way to the continuum limit of the Gross-Neveu solitary wave. However, contrary to what is the case for the DNLS, the two-site solution turns out to be stable close to the AC limit, while the three-site solution is the unstable one close to that limit. A count of the relevant eigenvalues near the AC limit is systematically given for these different cases. Subsequently a near-alternation of stability is observed between these two modes (the site- and inter-site-centered ones) that is somewhat reminiscent of the phenomenology identified in the saturable DNLS model [42, 43]. This is explored systematically, as is the feature of both of these solutions in producing a complex quartet of modes in a suitable band of the continuous spectrum. This oscillatory instability and its dynamical by-products are traced as a function of the propagation constant $\Lambda$ and of the inter-site coupling strength $\epsilon$. The dynamical manifestation of the instabilities within the discrete model is shown to lead to different possible features, including the potential mobility of the solitary waves or their splitting into multiple solitary waves of lower amplitude (and potentially of a different type).

Our presentation is structured as follows. In section II, we present an overview of our discrete model and its basic properties. In section III, we examine the different solutions in the vicinity of the AC limit. In section IV we examine the same solutions for large $\epsilon$, i.e., in the vicinity of the corresponding continuum limit. Finally, in section V, we explore the dynamical instability manifestations of the different solutions. Section VI summarizes our findings and presents our conclusions.

## II. MODEL AND THEORETICAL SETUP

The NLDE model that we will consider is the massive Gross-Neveu model with scalar-scalar interactions and a general power-law nonlinearity. This is motivated by recent corresponding continuum model explorations both at the level of mathematical analysis [16] and at that of numerical computations [18, 19]. The discrete version of the equation introduced herein will be based on a centered difference approximation of the first derivative in the form:

$$\begin{aligned} i\dot{U}_n &= \epsilon\nabla V_n - g(|U_n|^2 - |V_n|^2)^k U_n + mU_n, \\ i\dot{V}_n &= -\epsilon\nabla U_n + g(|U_n|^2 - |V_n|^2)^k V_n - mV_n, \end{aligned} \tag{1}$$

with $U_n$ and $V_n$ being the components of the spinor $\Psi_n \equiv (U_n, V_n)$ and $\nabla\Psi_n \equiv (\Psi_{n+1} - \Psi_{n-1})$ being the discrete gradient, with a centered difference scheme, as indicated above. The connection to the corresponding continuum limit can be assigned by selecting $\epsilon = 1/(2h)$ with $h$ being the lattice spacing (discretization parameter). It should also be noted in passing that we attempted to discretize by a forward difference scheme, but in the latter case solitary waves could only be found for small values of $\epsilon$ (i.e. large $h$) and could not be continued in a smooth fashion towards the continuum limit. Given also that the centered difference scheme is a higher order discrete approximation to the corresponding continuum limit and one whose solutions were identified in our computations below to experience a smooth transition into their continuum analogs, we therefore will only present results by means of the centered difference discretization scheme in what follows.

Our main focus hereafter will be on stationary solutions and their stability. Such solutions can be found by using $U_n(t) = \exp(-i\Lambda t)u_n$, $V_n(t) = \exp(-i\Lambda t)v_n$, and satisfy the coupled algebraic equations:

$$\begin{aligned} \epsilon\nabla v_n - g(|u_n|^2 - |v_n|^2)^k u_n + (m - \Lambda)u_n &= 0, \\ \epsilon\nabla u_n - g(|u_n|^2 - |v_n|^2)^k v_n + (m + \Lambda)v_n &= 0. \end{aligned} \tag{2}$$

Analogously to its continuum counterpart, the dynamical system of Eq. (1) presents a number of conserved quantities, such as the charge (squared $\ell^2$ norm):

$$Q = \sum_n \rho_n, \qquad \rho_n = |U_n|^2 + |V_n|^2, \tag{3}$$

with $\rho_n$ being the charge density, and the Hamiltonian:

$$H = \frac{1}{2}\sum_n \left[ (U_n^* \nabla V_n - V_n^* \nabla U_n) - \frac{g}{k+1}(|U_n|^2 - |V_n|^2)^{k+1} + m(|U_n|^2 - |V_n|^2) \right]. \tag{4}$$

The dynamical equations (1) can be derived from the Hamiltonian (4) by means of the Hamilton's equations:

$$\mathrm{i}\dot{U}_n = \frac{\delta H}{\delta U_n^*}, \qquad \mathrm{i}\dot{V}_n = \frac{\delta H}{\delta V_n^*}. \tag{5}$$

Once stationary solutions of the algebraic system of Eqs. (2) are calculated (by e.g. fixed points methods), their linear stability is considered by means of a Bogoliubov-de Gennes linearized stability analysis. More specifically, considering small perturbations [of order $\mathrm{O}(\delta)$, with $0 < \delta \ll 1$] of the stationary solutions, we substitute the ansatz

$$U_n(t) = e^{-i\Lambda t}\left[ u_{n,0} + \delta(a_n e^{i\omega t} + c_n^* e^{-i\omega^* t}) \right], \quad V_n(t) = e^{-i\Lambda t}\left[ v_{n,0} + \delta(b_n e^{i\omega t} + d_n^* e^{-i\omega^* t}) \right] \tag{6}$$

into Eqs. (1), and then solve the ensuing [to $\mathrm{O}(\delta)$] eigenvalue problem:

$$\omega \begin{pmatrix} a_n \\ b_n \\ c_n \\ d_n \end{pmatrix} = \mathcal{M} \begin{pmatrix} a_n \\ b_n \\ c_n \\ d_n \end{pmatrix}, \tag{7}$$

with $\mathcal{M}$ being

$$\mathcal{M} = \begin{pmatrix} \Lambda + J_n + L_n(u,u^*) & -\nabla - L_n(u,v^*) & L_n(u,u) & -L_n(u,v) \\ \nabla - L_n(u^*,v) & \Lambda - J_n + L_n(v,v^*) & -L_n(u,v) & L_n(v,v) \\ -L_n(u^*,u^*) & L_n(u^*,v^*) & \Lambda - J_n - L_n(u,u^*) & \nabla + L_n(u^*,v) \\ L_n(u^*,v^*) & -L_n(v^*,v^*) & -\nabla + L_n(u,v^*) & \Lambda + J_n - L_n(v,v^*) \end{pmatrix} \tag{8}$$

for the eigenvalue $\omega$ and associated eigenvector $\{(a_n, b_n, c_n, d_n)^T\}$. Here, $L_n(x,y)$ is a function defined as:

$$L_n(x,y) = k\chi_n^{k-1} x_{n,0} y_{n,0}\ , \tag{9}$$

with $J_n$ being:

$$J_n \equiv g\chi_n^k - m\ , \tag{10}$$

and

$$\chi_n \equiv |u_{n,0}|^2 - |v_{n,0}|^2. \tag{11}$$

The dispersion relation of the linear excitations corresponds to the continuous spectrum that will be identified in the linearization around the trivial $u_n = v_n = 0\ \forall\ n$ solution. This relation can be identified by decomposing the perturbations as $\{a_n, b_n, c_n, d_n\} = \{A, B, C, D\}\exp(iqn)$ in Eqs. (2) and deriving the resulting condition:

$$\omega(q) = \pm\Lambda \pm \sqrt{m^2 + 4\epsilon^2 \sin^2 q}. \tag{12}$$

Consequently, several distinguished regions can be identified in the essential spectrum: for $\omega \in [-\Lambda - m, \Lambda - m] \cup [-\Lambda + m, \Lambda + m]$, function $\omega(q)$ acquires the relevant values for a single value of its argument (within its domain of periodicity), whereas this function acquires the values of $\omega \in [-\sqrt{m^2 + 4\epsilon^2}, \Lambda - m] \cup [-\Lambda + m, \sqrt{m^2 + 4\epsilon^2}]$ for two separate values of its argument (within its domain of periodicity). The limits of the former region are denoted as embedded thresholds (cf. [11]). For the sake of simplicity, we denoted the former region by $\omega_1$, and the latter by $\omega_2$.

In what follows, for concreteness we will set $m = g = 1$ (as this choice can be made by renormalizing $\epsilon$, the time and the wave function) and vary $\Lambda$, as well as $\epsilon$, as our relevant parameters.

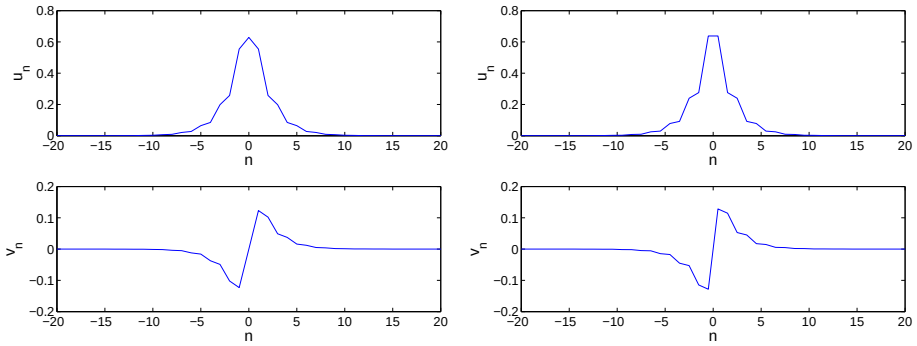


FIG. 1: (Left) The two-component profiles for a 3-site soliton with $\Lambda = 0.8$ and $\epsilon = 0.5$ (i.e. close to the anti-continuum limit). Right panels shows the profile for the complementary 2-site soliton with the same parameters.

## III. RESULTS FROM THE ANTI-CONTINUUM LIMIT (SMALL COUPLING REGIME)

In this section, we consider the existence, stability and dynamics of discrete solitons from the anti-continuum ($\epsilon = 0$) to the continuum ($\epsilon \to \infty$) limit.

We start by considering the three-site soliton, which in the anti-continuum (AC) limit is given by $v_n = 0 \; \forall \; n$ and $u_{-1} = u_0 = u_1 = (1-\Lambda)^{1/(2k)}$, $u_n = 0 \; \forall \; |n| \geq 2$ [see Fig. 1 (left panel)]. The motivation for starting with this particular solution, as opposed to the more "canonical" single site one, is that this is the state that is found by extending the continuum solitary wave [cf. Eq. (14) below] all the way to the AC limit. We will, however, discuss the continuation of the single-site (and the 2-site) solution in detail in what follows.

Let us explain below the general behavior for $\Lambda > 1/3$. Outside this range, the solitary waves are generically (i.e., except for very narrow stability bands) unstable and hence we do not consider them further here.

In the AC limit the individual sites are decoupled, and the eigenvalues of their respective $4 \times 4$ matrices can be explicitly computed for both the cases of excited and non-excited sites. Thus it is straightforward to see from (8) that in that limit and for any value of $k$, this three-site solution possesses 3 pairs of modes at $\omega = 0$, 3 pairs at $\omega = \pm 2\Lambda$, $(N-3)$ pairs at $\omega = \pm(1+\Lambda)$ and $(N-3)$ pairs at $\omega = \pm(1-\Lambda)$. When the coupling is switched on (see Fig. 2), the wave becomes exponentially unstable because of one among the 3 pairs at $\omega = 0$ that detaches from the origin yielding an imaginary eigenfrequency pair in a similar way as occurs e.g. for the two-site structure in the DNLS equation [5]. The other two vanishing eigenfrequency pairs remain at the origin. In addition, the eigenmodes at $\omega = \pm 2\Lambda$ detach into three pairs that will subsequently collide with the essential spectrum; let us denote those modes as A, B, C (from upper to lower real part of the eigenfrequency). Mode C remains exactly at $\omega = \pm 2\Lambda$ for every coupling. Notice that mode C is always below the essential spectrum for $\Lambda < 1/3$. The real part of the eigenfrequency of mode A rapidly increases entering $\omega_2(q)$ at the point where the imaginary part of the eigenmode responsible for the exponential instability reaches its maximum. The exponential instability mentioned previously disappears close to (but not at) the point where mode C enters $\omega_1(q)$. However, when the coupling increases, the exponential instability appears again with a similar (non-monotonic) behavior as the previous one, except for the presence of smaller growth rates and of a slower decrease in the growth rate (past the point of the maximal growth rate). The most complex parametric dependence is the one experienced by mode B. The latter enters $\omega_1(q)$ for a value of $\epsilon$ higher than that for which mode C enters therein. Then, the system becomes oscillatorily unstable and undergoes a Hopf bifurcation [in the case of finite systems, due to the quantization of the continuous spectrum, this translates into a series of instability bubbles; for a similar scenario in the DNLS see e.g. [45]]. As a consequence, there are many oscillations in the imaginary part of mode B when the coupling is high; the amplitude of those oscillations decreases when the system size increases, as shown in the inset of bottom right panel of Fig. 2. When the frequency increases (say $\Lambda \gtrsim 0.67$) the imaginary part of mode B does not asymptote to a nearly constant value as the coupling strength increases, but, on the contrary, a series of oscillation bubbles around 0 appears (see top panels of Fig. 2). The persistence of those oscillations in the continuum limit will be considered in Section IV (see also Fig. 12 therein).

A more complete scenario of the linearization eigenfrequencies is presented in Fig. 3, where the largest imaginary part of eigenfrequencies with zero and non-zero real part (i.e. responsible for exponential and Hopf bifurcations, respectively), with respect to $\epsilon \leq 2.5$ and $1/3 \leq \Lambda < 1$ is presented. A cut-off for growth rates smaller than $10^{-3}$ for Hopf bifurcations and $10^{-6}$ for bifurcations leading to exponential instabilities has been introduced. It can be observed that the instability bubbles emerge in the right panel for $\Lambda \gtrsim 0.67$ and $\epsilon \gtrsim 1.08$. In addition, it is observed that exponential instabilities emerge in several lobes, which suggests a cascading mechanism of destabilizations and restabilizations that we will return to below, upon examination of the two-site solitary wave.

A complementary scenario is experienced by the two-site solitary wave, given in the AC limit by $v_n = 0 \; \forall \; n$ and $u_0 = u_1 =$

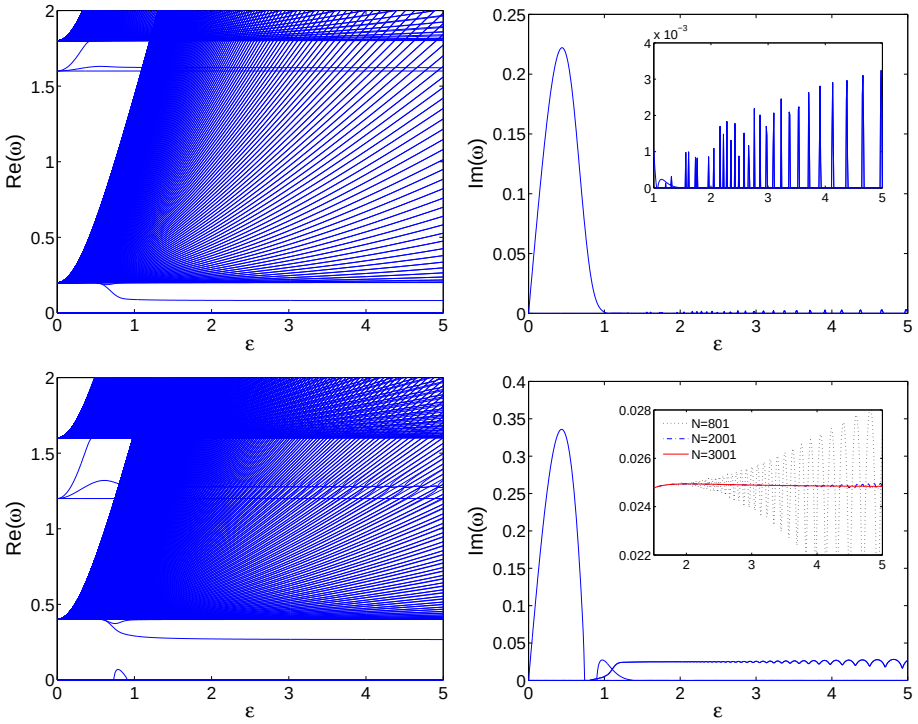


FIG. 2: Spectrum of the stability matrix (8) for discrete NLDE 3-site solitons with $\Lambda = 0.8$ (top) and $\Lambda = 0.6$ (bottom). The imaginary (right) and real (left) parts of the corresponding eigenfrequencies are shown as a function of the coupling strength $\epsilon$. Only the positive real and imaginary parts of the eigenfrequencies are shown. The size of the system is $N = 801$. In the top right, the inset is a magnification of the relevant Im$(\omega)$ shown in the figure but at a different scale. The inset in the bottom right panel shows the oscillations of the growth rate for different system sizes when $\Lambda = 0.6$. Notice that oscillation amplitude decreases rapidly as the number of lattice nodes increases.

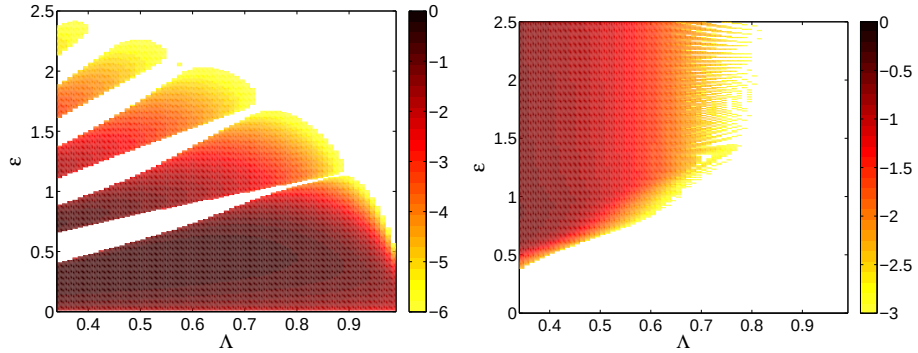


FIG. 3: Logarithm of the largest imaginary part of eigenvalues with zero (left) and non-zero (right) real part with $N = 801$. Blank areas correspond to stable solitons.

$(1-\Lambda)^{1/(2k)}$, $u_n = 0$ elsewhere [see Fig. 1 (right panels)]. At this limit, the 2-site structure possesses 2 pairs of modes at $\omega = 0$, 2 pairs at $\omega = \pm 2\Lambda$, $(N-2)$ pairs at $\omega = \pm(1+\Lambda)$ and $(N-2)$ pairs at $\omega = \pm(1-\Lambda)$. When the coupling is switched on (see Fig. 4), the structure remains stable because of the persistence of both pairs at $\omega = 0$. Mode A from $|\omega| = 2\Lambda$ does not exist for this case; on the other hand, the oscillatory instabilities caused by mode B also exist for the 2-site case. When increasing the coupling, the soliton experiences a bifurcation leading to an exponential instability and becomes unstable, contrary to the 3-site soliton (notice that in typical Klein-Gordon and –e.g. saturable– DNLS settings, such stability exchanges take place between 2-site and 1-site breathers or solitons [42–44]). Here, there are exponential stability exchanges between 2-site and 3-site solitons, although the bifurcations of the two families of solutions do not perfectly coincide (nevertheless, in a number of such exchanges, the corresponding stabilization/destabilization thresholds are fairly proximal). This scenario is summarized in Fig. 5. We should note in passing that these near-exchanges of stability suggest a scenario similar to the ones occurring e.g. in the

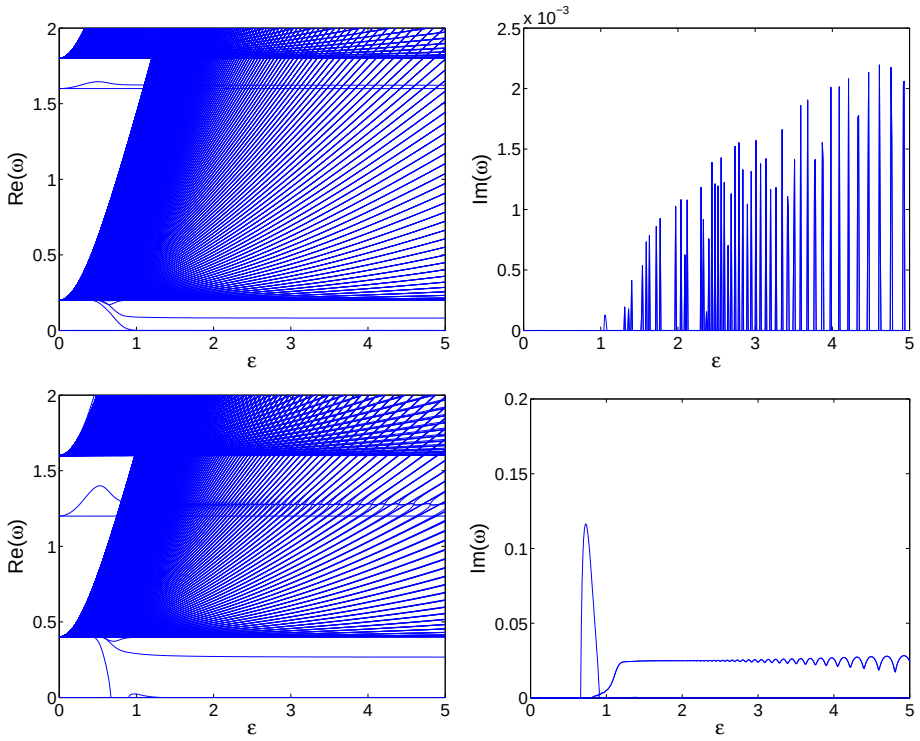


FIG. 4: Same as Fig.2 but for the discrete NLDE 2-site solitons with $\Lambda = 0.8$ (top) and $\Lambda = 0.6$ (bottom).

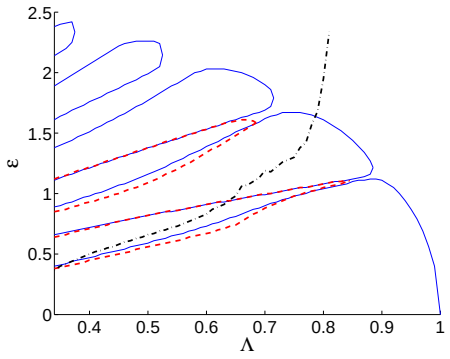


FIG. 5: $\epsilon$ vs $\Lambda$ plane where different unstable regimes for 3-site and 2-site solitons are displayed. 3-site solitons are unstable inside the full line regions, whereas unstable 2-site solitons are inside dashed lines. Above the dashed-dotted lines, both solutions are oscillatorily unstable.

saturable or cubic-quintic DNLS model where the near-exchange of stability of the 1- and 2-site solitary waves (in that case) is mediated through a series of pitchfork and reverse pitchfork bifurcations of asymmetric solution branches [46, 47]. However, we will not pursue the relevant narrow branches of asymmetric solutions herein.

There is an interesting kind of solution that also exists from the AC limit and can be extended all the way to the continuum limit, namely the one-site soliton [see Fig. 6 (left panels)]. This has the following property which is, in fact, preserved upon continuation for any value of the coupling (see Fig. 7): $u_n = 0$ for odd $n$ and $v_n = 0$ for even $n$; however, the charge density of the soliton is qualitatively different from that of the three-site solitons. In the AC limit $\epsilon = 0$, $u_0 = (1 - \Lambda)^{1/(2k)}$, and $u_n = 0$ for the rest of sites (with $v_n = 0 \; \forall \; n$).

The form of this solution can be identified as we approach the continuum limit as $u_n = 0$ for odd $n$ and $v_n = 0$ for even $n$, by transforming the discrete NLDE equation (1) into the new set of equations:

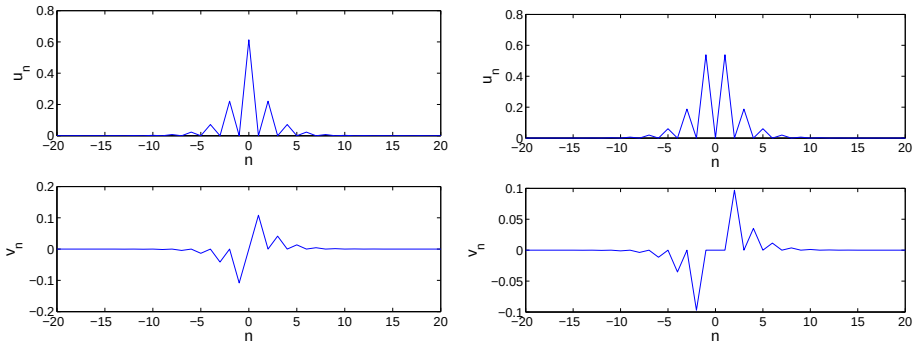


FIG. 6: Same as Fig. 1 but for a 1-site soliton (left) and its complementary solution (right), which possesses a hole at $n = 0$.

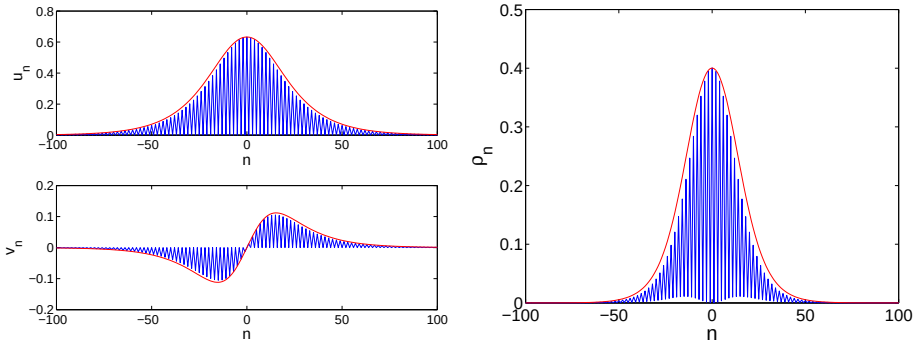


FIG. 7: (Left) The two-component profiles for a 1-site soliton (blue) and a 3-site soliton (red) with $\Lambda = 0.8$ at $\epsilon = 5$. (Right) Charge density $\rho_n = |u_n|^2 + |v_n|^2$ for the solitary wave at the left. It is clear that the 1-site soliton does *not* asymptote to the 3-site soliton, but rather to a different envelope that will be revealed in section IV below. Notice also that the 2-site soliton is obtained by a translation of $n = 1/2$ to the 3-site soliton and has the same continuum limit envelope.

$$\begin{aligned} \epsilon(v_{n+1} - v_{n-1}) - g u_n^{2k+1} + (m - \Lambda) u_n &= 0, \text{ for even } n \\ \epsilon(u_{n+2} - u_n) - (-1)^k g v_{n+1}^{2k+1} + (m + \Lambda) v_{n+1} &= 0, \text{ for even } n \end{aligned} \tag{13}$$

which possesses homoclinic solutions in the continuum limit (see Section IV).

The spectrum of the one-site solitons at $\epsilon = 0$ consists of a single pair of eigenvalues at $\omega = 0$ and another single pair at $\omega = \pm 2\Lambda$; apart from these, there are $N - 1$ pairs at $\omega = \pm(1 + \Lambda)$ and $\omega = \pm(1 - \Lambda)$. When the coupling is switched on, as there is only a single pair of eigenmodes at $\omega = 0$, the soliton does not experience exponential instabilities; in addition, the non-existence of mode B prevents the existence of destabilizing Hopf bifurcations arising in 3-site and 2-site solitons (see Fig. 8). The only observed instability is an exponential one arising for a finite value of coupling and caused by a mode that bifurcates from the essential spectrum as the coupling strength increases; the growth rate which has a non-monotonic dependence on the coupling and tends asymptotically to zero when reaching the continuum limit, and its maximum value decreasing with $\Lambda$ (for fixed coupling) are shown in Fig. 9 for more details. Similar to the 3-site structures, there is a complementary family of solitons consisting of 2-site structures with a hole in between, characterized by $u_0 = u_2$ [see Fig. 6 (right panels)].

Let us finally mention the existence of a family of solutions with $\Lambda < 0$, which possesses $u = 0$ at the AC limit; the nonzero values of $v$ at this limit are given by $(1 + \Lambda)^{1/2k}$. This solution can be transformed into that with $-\Lambda$ by virtue of $u_n \to v_n$, $v_n \to u_n$ and $g \to (-1)^k g$ as long as $k \in \mathbb{N}$.

## IV. RESULTS NEAR THE CONTINUUM LIMIT (LARGE COUPLING REGIME)

In this section, on one hand, we will connect the findings of our model with some previous results about the stability of the continuous NLDE. On the other hand, we will perform the Bogoliubov-de Gennes (BdG) spectral stability analysis of the discrete NLDE for a large coupling such as $\epsilon = 5$, which corresponds to a spatial discretization parameter $h = 0.1$.

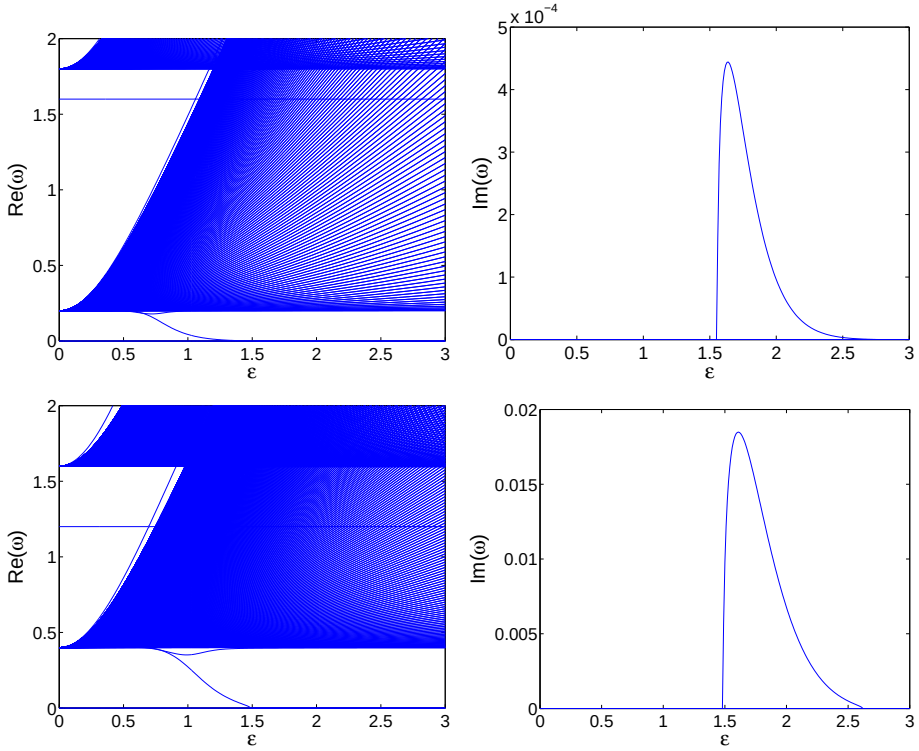


FIG. 8: Same as Fig.2 but for discrete NLDE 1-site solitons with $\Lambda = 0.8$ (top) and $\Lambda = 0.6$ (bottom).

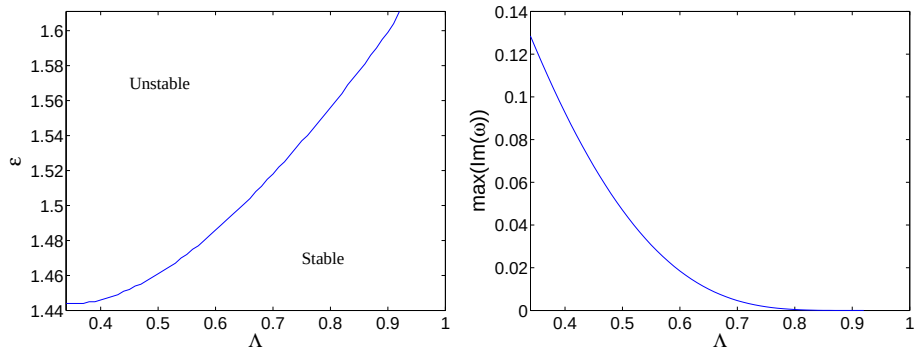


FIG. 9: Exponential instability loci (left) for a 1-site soliton are shown in the $\epsilon$-$\Lambda$ plane in the left panel. The right panel shows the maximum (over the considered $\epsilon$ variations) growth rate at each value of $\Lambda$. For $\Lambda > 0.92$, the growth rates for the 1-site soliton are smaller than $10^{-7}$ and cannot be accurately traced because of machine precision.

Previous results from Comech (see Refs. [11, 48–50]) show that close to the non-relativistic limit ($\Lambda \lesssim 1$), the Vakhitov–Kolokolov criterion should hold. Based on it [49], it is concluded that no unstable eigefrequency should emerge from $\omega = 0$ close to this limit for $k = 1$ or $k = 2$ (contrary to the $k \geq 3$, $k \in \mathbb{N}$ case where a pair of eigenfrequencies with a nonzero imaginary part and a zero real part are present) and, consequently, no exponential instability should exist in that limit. Additionally, for any $k$, the existence of an eigenfrequency $|\omega| = 2\Lambda$ is also predicted. This mode enters the linear mode band at $\Lambda = 1/3$ (when increasing $\Lambda$).

The work of [20], based on the so-called Bogolubsky criterion, suggests that solitary waves are always unstable for $\Lambda < \Lambda_c$. [It is worth noting here that the criterion mentioned above is able to give a necessary condition and, consequently, the minimum value for which solitons are stable must be determined numerically]. In the cubic case ($k = 1$) it is predicted in [20] that $\Lambda_c = 0.6976$. However, in a recent paper [19], further numerical simulations have suggested that solitons may be dynamically stable for $\Lambda \geq 0.56$. Despite the existence of a detailed review on computational methods about evolutionary dynamics in nonlinear Dirac equations [51], the continuum limit stability still remains rather controversial. The recent work of [52] concurs with the earlier work of Comech and collaborators above in finding the $k = 1$ soliton as linearly stable for all values of $\Lambda$.

Our own continuum computations using a Chebyshev interpolation method are, in fact, in agreement with this conclusion. Yet, clearly this poses a question regarding the nature of instability in recent numerical and dynamical observations [19, 20] and also how the observations herein for large (but finite) $\epsilon$ (small –but finite– $h$) can be reconciled with the above continuum features. This is a particularly challenging open problem that merits considerable future study.

The analytical form of the profile of solitons in the continuum limit is given by [18, 20]:

$$u(x)=\sqrt{\frac{(1+\Lambda)\cosh^2(k\beta x)}{1+\Lambda\cosh(2k\beta x)}}\left[\frac{(k+1)\beta^2}{1+\Lambda\cosh(2k\beta x)}\right]^{1/2k},\quad v(x)=\sqrt{\frac{(1-\Lambda)\sinh^2(k\beta x)}{1+\Lambda\cosh(2k\beta x)}}\left[\frac{(k+1)\beta^2}{1+\Lambda\cosh(2k\beta x)}\right]^{1/2k}, \tag{14}$$

with $\beta=\sqrt{1-\Lambda^2}$. When $k=1$ the equations above can be simplified to:

$$u(x)=\frac{\sqrt{2(1-\Lambda)}}{[1-\mu\tanh^2(\beta x)]\cosh(\beta x)},\quad v(x)=\frac{\sqrt{2\mu(1-\Lambda)}\tanh(\beta x)}{[1-\mu\tanh^2(\beta x)]\cosh(\beta x)}, \tag{15}$$

with $\mu=(1-\Lambda)/(1+\Lambda)$. As demonstrated in [18], continuous solitons become double-humped for $\Lambda$ smaller than a critical value for every $k$. Fig. 10 shows the profile and spectral planes for two different examples of solitons close to the continuum limit with $k=1$.

We show in Fig. 11 the stability eigenvalues for $k=1$ in a domain $x\in[-L/2,L/2]$, with $L=80$ and a discretization step $h=0.1$. Although there are instabilities caused by eigenvalue collisions in the part of the spectrum associated with $\omega_2(q)$, we have neglected them, as they disappear in the limit of $h\to 0$ and $L\to\infty$. The waves are found to be unstable for small $\Lambda$, with a growth rate that decreases when $\Lambda$ is increased. The source of instabilities is a localized mode (with non-zero imaginary part of its eigenfrequency even when $\Lambda\to 0$) that enters $\omega_1(q)$ at $\Lambda\approx 0.037$ i.e. it embeds into the essential spectrum. Once inside the linear modes band, this localized mode causes multiple bubbles, yet at $\Lambda\approx 0.632$, it returns to the real eigenfrequency axis and the solitary wave becomes stable. Nevertheless, this stability is ephemeral, as the soliton becomes unstable again at $\Lambda\approx 0.634$. From this point, there is a succession of instability bubbles, whose amplitude (i.e., the maximal growth rate associated with them) decreases with $\Lambda$. Notice also the existence of the eigenvalue with $\omega=2\Lambda$, which embeds into the spectrum, i.e. enters $\omega_1(q)$ at $\Lambda=1/3$.

In order to observe the behavior of bubbles when the domain is enlarged, we have included Fig. 12 where the growth rate is plotted for $L=80$, 200 and 300. It is observed that the number of bubbles increases with $L$, but their width decreases. In any case, the envelope of the bubbles tends to zero asymptotically when $\Lambda$ approaches 1, in a similar way as it was observed for dark solitons in DNLS settings [45]. Unfortunately, the convex nature of the relevant (apparent) envelope curve is inconclusive in connection to the stability aspect. In particular, it is unclear, based on the present computations, whether the curve, as $h\to 0$, *still* intersects the axis and no longer features an unstable mode past a critical $\Lambda_c$, as is the case with our finite $h$, finite domain computations in Fig. 12. The alternative scenario is that the approach to the stable NLS limit of $\Lambda\to 1$ (a glimpse of which is illustrated in Fig. 12) is merely asymptotic. It would be especially interesting to pursue this intriguing aspect further, pushing the envelope of the currently available numerical tools.

As mentioned in Section III, the 1-site solitons can also exist in the continuum limit. There, by neglecting the irrelevant (in this setting) inactive odd sites for one of the fields, and the even ones for the other, the envelope of the solitary waves can be seen to approach the homoclinic orbits of the following system of ODEs that is found by obtaining the continuum limit of (13):

$$\begin{aligned}\partial_x u &= (-1)^k g v^{2k+1}-(m+\Lambda)v,\\ \partial_x v &= g u^{2k+1}-(m-\Lambda)u.\end{aligned} \tag{16}$$

Using phase plane numerical analysis (not shown here), we have confirmed that Eqs. (16) possess a homoclinic orbit in the case of $g=m=1$ and $k=1$, for a wide range of $\Lambda$'s. We have also confirmed that it is at these very homoclinic orbits that the envelope of our NLDE 1-site solution tends to as the coupling strength is increased although an explicit analytical form for these is not presently available.

As a final comment regarding the stability analysis, we note that our approach allows to examine not only the variations as a function of the propagation constant $\Lambda$, as well as the coupling strength $\epsilon$, but additionally also with respect to the nonlinearity exponent parameter $k$. Fig. 13 shows some typical examples of this variation for $h=0.1$ and values of $\Lambda=0.5$ (top) and $\Lambda=0.8$ (bottom). The parametric variation of $k$ reveals both the Hopf and exponential instabilities of the system. As regards the latter, we note that for sufficiently high values of $k$, an eigenfrequency bifurcating from the continuous spectrum crosses the spectral plane origin becoming imaginary, in accordance with the expectation that for sufficiently high $k$ a blow-up type instability (which for $\Lambda\to 1$, i.e., the NLSE limit, should occur for $k>2$) should emerge. The relevant critical points are $k=3.35$ and $k=2.36$, respectively for the considered values of $\Lambda$ of 0.5 and 0.8. On the other hand, another interesting observation is that a similar bifurcation to exponential instability appears to emerge in the small positive $k$ i.e., the weakly

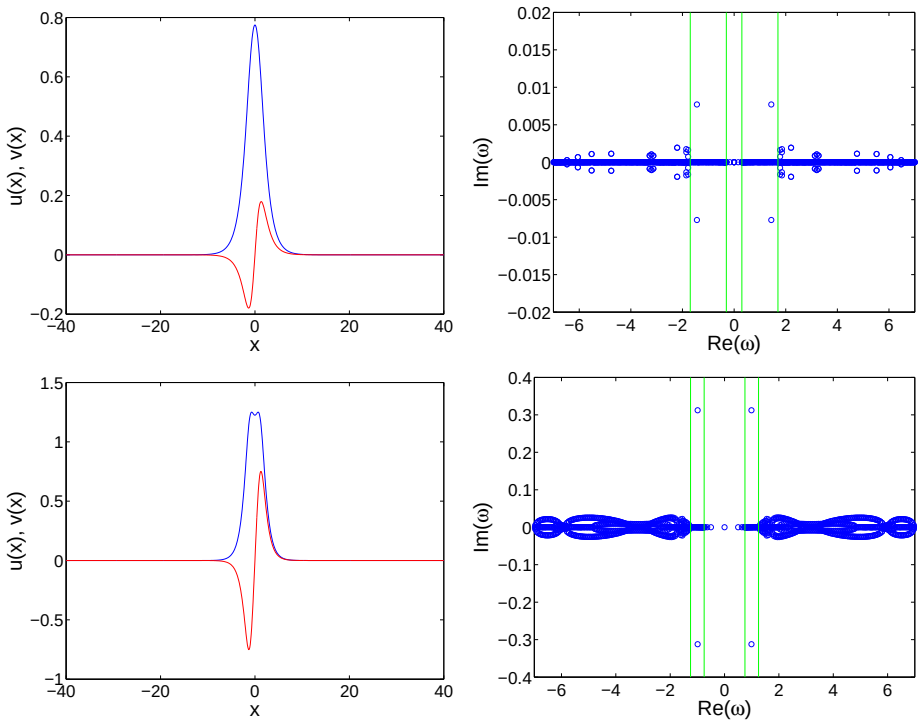


FIG. 10: (Left) Solitary wave profiles and (right) spectral planes for $h = 0.1$, $L = 80$ and $\Lambda = 0.7$ (top) and $\Lambda = 0.25$ (bottom). Lines in the right figures indicate the location of the embedded thresholds of the essential spectrum. Instabilities for $\mathrm{Re}(\omega) \in \omega_2(q)$, i.e. beyond the embedded thresholds, should vanish when $L \to \infty$.

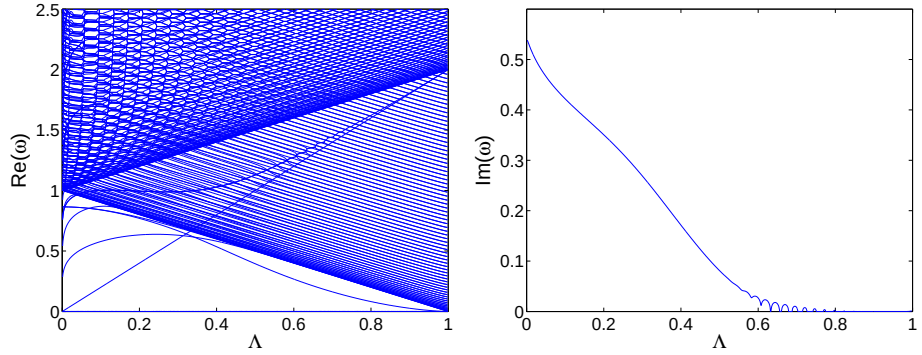


FIG. 11: Spectrum of the stability matrix (8) for solitons with $h = 0.1$ and $L = 80$. For the sake of simplicity, only the positive real and imaginary parts of the eigenvalues are shown.

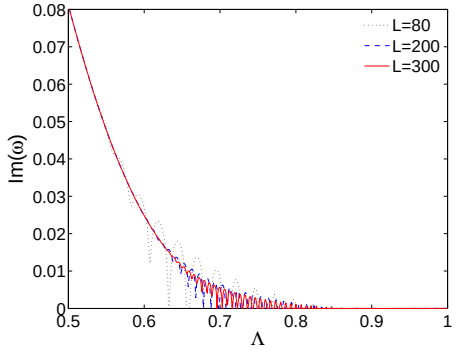


FIG. 12: Dependence of the growth rates of the solitary waves shown in Fig. 11 for different domain lengths. As $L$ increases, we progressively can discern the envelope of the infinite domain limit.

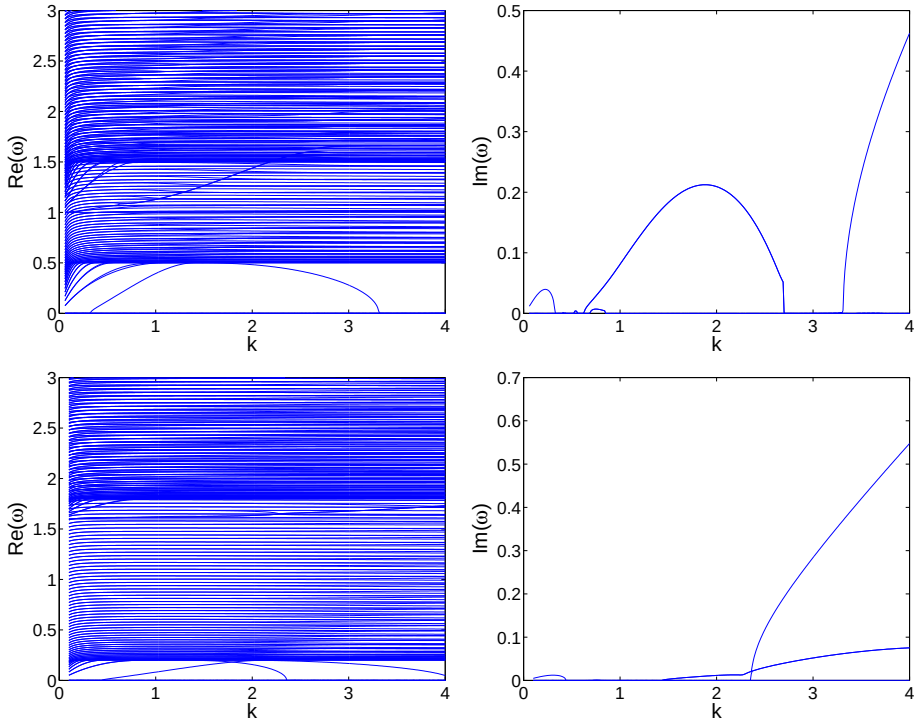


FIG. 13: Spectrum of the stability matrix (8) for solitons with $h = 0.1$ and $L = 80$. $\Lambda = 0.5$ in upper panels and $\Lambda = 0.8$ in bottom ones, in this case as a function of the nonlinearity exponent $k$. In the former case, exponential instabilities emerge for $k < 0.33$ and $k > 3.35$, whereas in the latter case, those instabilities take place for $k < 0.44$ and $k > 2.36$.

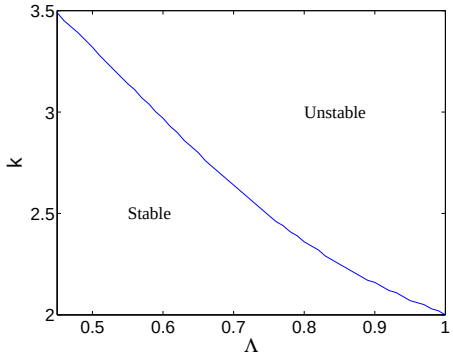


FIG. 14: $k$ vs $\Lambda$ plane where the behavior of solitons with respect to exponential instabilities is displayed. Notice that the critical value $k = 2$ is retrieved at the non-relativistic (NLSE) limit.

nonlinear limit. This instability arising for $k < 0.33$ and $k < 0.44$ in the top and bottom, respectively, panel of Fig. 13 is worth examining further in its own right, possibly through a perturbative calculation.

A systematic exploration of the $k$-$\Lambda$ plane of the relevant exponential instability is identified in Fig. 14. As expected in the non-relativistic NLSE limit of $\Lambda \to 1$, no exponential instabilities are observed when $k < 2$, whereas for $k > 2$, the solitons are unstable i.e., amenable to collapse. Naturally, genuine collapse phenomena can only arise in the continuum version of the model, while the discrete lattice dynamics can only feature a quasi-collapse phenomenon, where an abrupt decrease of the localization width and increase of the solution amplitude occurs. Clearly, in the latter case, the full collapse cannot occur as it is arrested by the presence of the lattice. We can see that as $\Lambda$ decreases from that limit, the corresponding critical $k$ for the instability monotonically increases.

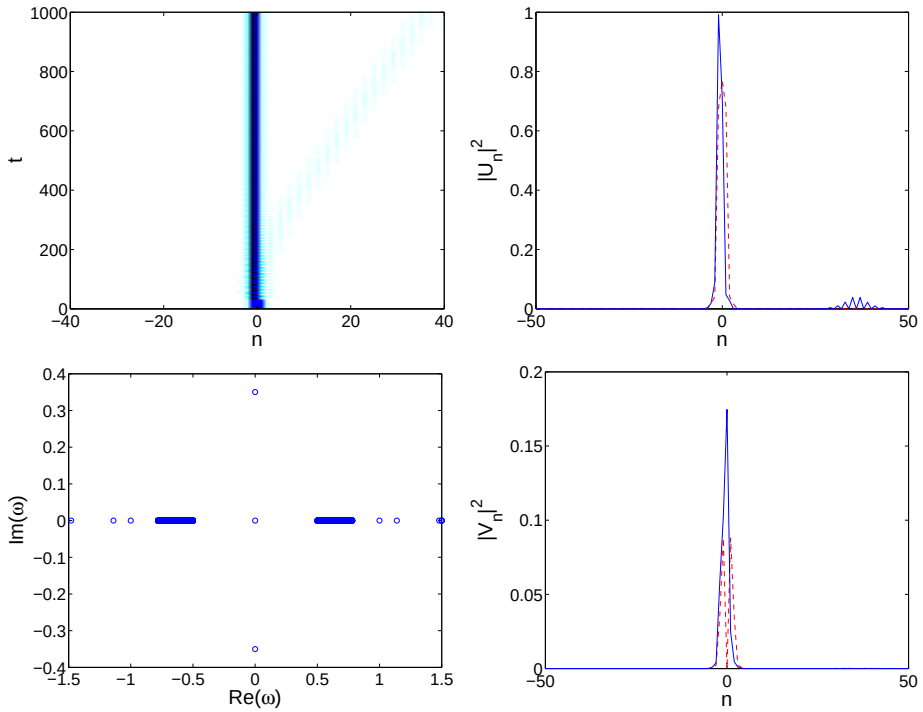


FIG. 15: Evolution of the soliton with $\Lambda = 0.5$ and $\epsilon = 0.4$. Top left panel shows the evolution of the charge density $\rho_n$. Right panels depict the fields at $t = 0$ (dashed line) and at $t = 1000$ (solid line). Bottom left panel displays the spectral plane of the solitary wave.

## V. DYNAMICAL EVOLUTION OF INSTABILITIES

We have also briefly analyzed the dynamics of unstable 3-site solutions in different regimes. Below, we give a number of selected results in connection to the relevant numerical evolution, although admittedly a systematic classification of the dynamical implications of the different identified instabilities and of the various possible configurations identified herein is a separate numerical project in its own right.

Fig. 15 shows the evolution of a solitary wave with $\Lambda = 0.5$ and $\epsilon = 0.4$, i.e. inside the lower lobe of exponential instabilities. We observe that the structure emits linear wave "radiation" and subsequently deforms towards a more compact configuration with fewer high-amplitude excited sites (more specifically one in each component). If a solution within the intermediate lobe is taken (as e.g. that of Fig. 16, where $\Lambda = 0.6$ and $\epsilon = 0.95$), it is observed that the soliton moves along the lattice. In this regime, both an exponential and an oscillatory instability are present. As the soliton traverses the lattice, in the presence of the well-known energy barrier that it needs to overcome to move by a lattice site (the celebrated, in dislocation and in discrete soliton theory, Peierls-Nabarro barrier [2, 5]), it gradually decelerates and eventually stops being trapped and nearly pinned on a lattice site. However, beyond that stage, the oscillatory instability of the standing wave takes over, resulting into an oscillatory expulsion of the wave from the pinned site, in fact moving in the opposite direction (and with a larger speed) than it originally did. It should be noted that examples of such "boomeronic" behavior have also been encountered in other discrete (non-momentum conserving) systems recently as well; see e.g. [53]. Generally, for cases of larger coupling, we find that the solutions are more prone to becoming mobile, upon the manifestation of the dynamical instability.

Fig. 17 depicts an oscillatorily unstable wave with $\Lambda = 0.6$ and $\epsilon = 2$. Interestingly, the latter splits into two daughter-waves as a result of the oscillatory growth; the asymmetry of these waves is caused by the amplification of round-off errors due to the presence of the instability. Once the original structure is split, the charge density at even sites is close to zero (a state similar to the 1-site soliton). That is, the offspring in this case belong to the same class of solitary waves as the 1-site solution examined above. If an oscillatory unstable soliton is taken within the region of oscillatory instability bubbles (see Fig. 18, where $\Lambda = 0.7$ and $\epsilon = 2$), the soliton is put into motion. Once again, this is a relatively common feature of case examples with large values of $\epsilon$ that are more proximal to the continuum limit of the problem. Notice, however, additionally that in the process of shedding away radiative wavepackets that manifests the dynamical instability and sets the solitary wave in motion, the amplitude of the structure decreases, which indicates that its effective $\Lambda$ increases and hence renders it more robust.

Lastly, we should note that we have also examined dynamical instabilities of other structures such as 1- and 2-site solitons. These often, too, result in mobile coherent structures, especially for large values of $\epsilon$, although some states, such as the staggered 1-site wave are less amenable to extensive traveling throughout the lattice, perhaps partly due to their special spatial structure.

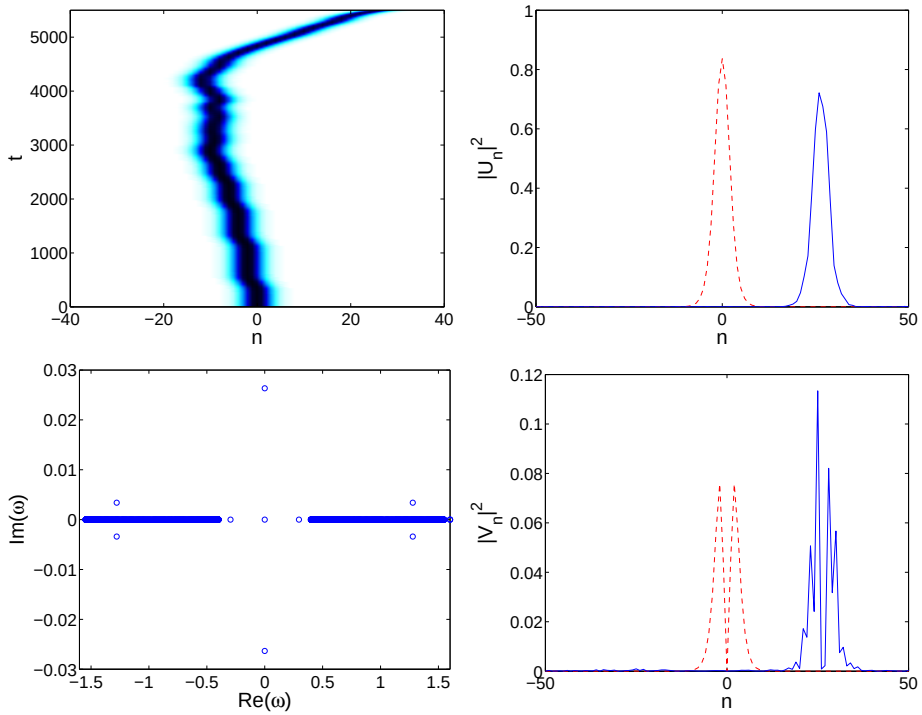


FIG. 16: Evolution of the soliton with $\Lambda = 0.6$ and $\epsilon = 0.95$. Top left panel shows the evolution of the charge density $\rho_n$. Right panels depict the fields at $t = 0$ (dashed line) and at $t = 5500$ (solid line). Bottom left panel displays the spectral plane of the solitary wave.

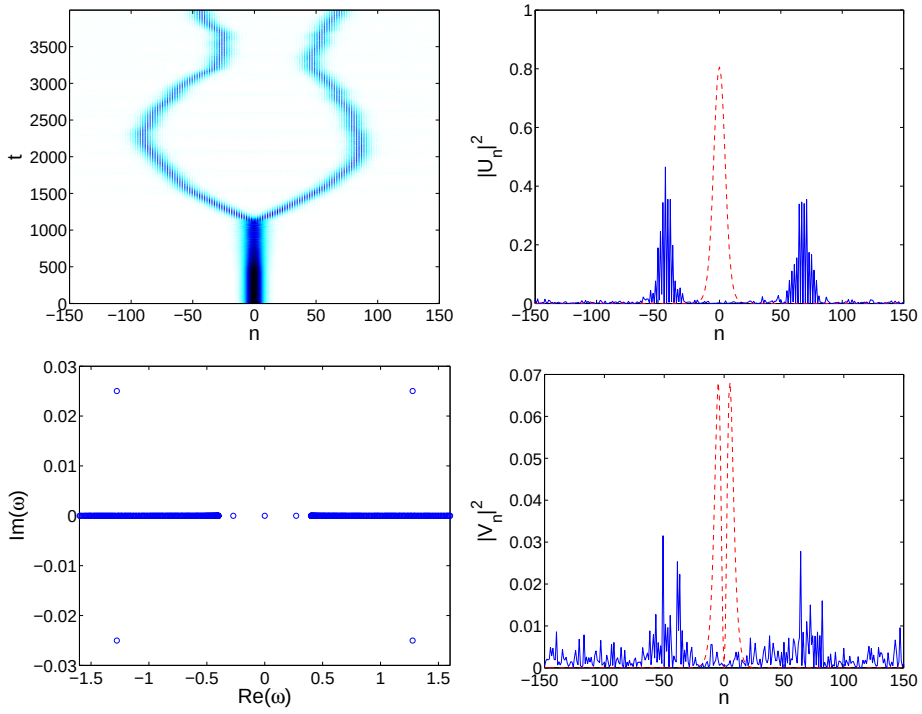


FIG. 17: Evolution of the soliton with $\Lambda = 0.6$ and $\epsilon = 2$. Top left panel shows the evolution of the charge density $\rho_n$. Right panels depict the fields at $t = 0$ (dashed line) and at $t = 4000$ (solid line). Bottom left panel displays the spectral plane of the solitary wave.

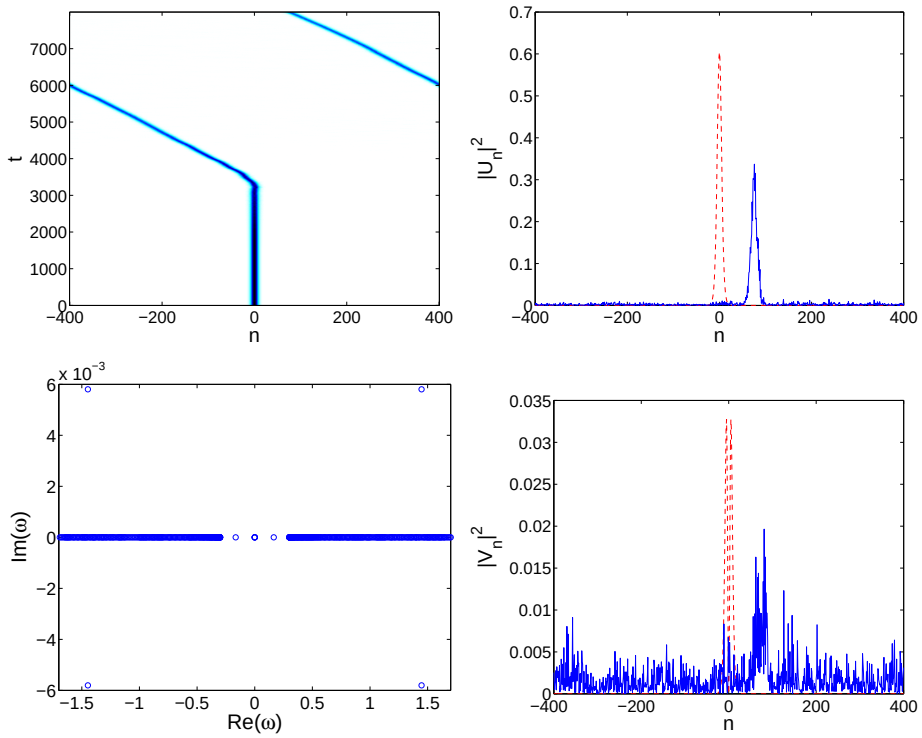


FIG. 18: Evolution of the soliton with $\Lambda = 0.7$ and $\epsilon = 2$. Top left panel shows the evolution of the charge density $\rho_n$. Right panels depict the fields at $t = 0$ (dashed line) and at $t = 8000$ (solid line). Bottom left panel displays the spectral plane of the solitary wave.

## VI. CONCLUSIONS AND FUTURE CHALLENGES

In the present work we have examined a lattice analogue of the nonlinear Dirac equation. Motivated by the considerable volume of both mathematical and computational investigations of the continuum limit of the corresponding problem, we have developed a prototypical discretization scheme whose continuum limit is the Gross-Neveu model. This is a model that while it does not presently possess a straightforward physical realization (e.g. analogous to what is the case for its DNLS analogue and, say, optical waveguide arrays [54]), it nevertheless is of substantial interest in its own right for a number of reasons. It is useful (and relevant to understand), on one hand, as a numerical scheme and a computational tool for approximating the corresponding continuum limit (in regimes of large coupling strength $\epsilon$). On the other hand, its analytical tractability in the vicinity of the anti-continuum limit of uncoupled sites makes it a useful starting point for the exploration of the spectral properties of solitary waves. In the AC limit, there is a complete control over these spectral properties and corresponding eigenvalues. Starting from this point, continuation over the coupling strength $\epsilon$ can be used in order to understand both the features of the discrete model and those of its continuum limit. Moreover, the physical realization of quasi-discrete systems possessing Dirac-like dynamics such as spin-orbit Bose-Einstein condensates in the presence of optical lattices very recently [40], seems to strongly suggest the potential experimentally-relevant realization of models of this class in the near future.

In light of the above motivations, here we have shown a multitude of unexpected properties that merit further studies not only from a computational but also importantly from a rigorously mathematical point of view. In particular, we showed that a single site excitation does not continue, as might be expected, to a continuum solitary wave of the Gross-Neveu model. Instead, it forms a remarkable staggered structure that approaches in the limit of $\epsilon$ large (while being preserved as a state) the envelope of the homoclinic orbit of a different dynamical model. This appears to be a fairly robust structure in its parametric dependence over $\epsilon$ and $\Lambda$. On the other hand, the two- and three-site initial excitations play the role, respectively, of the one- and two-site excitations of the DNLS. Yet, here a situation more akin to the saturable analogue of the DNLS occurs [42, 43], whereby exchanges of stability between the on-site and inter-site solutions arise. Likely, and analogously to corresponding DNLS cubic-quintic or saturable settings, these exchanges are mediated by pitchfork bifurcations (and reverse pitchforks) generating asymmetric waveforms, a topic potentially worthy of further investigation in the future. Additionally, these states appear to possess quartet of eigenfrequencies chiefly responsible for their instability. While this instability appears to reach an asymptotic growth rate (over $\epsilon$ variations) for values of $\Lambda$ below a critical one, the fate of this instability as the continuum limit of the problem is approached is, indeed, an open problem, as per our earlier discussion. In that connection, it is relevant to point out that we have observed the manifestation of the instability to potentially lead to traveling and mobility of the structure, while in other cases,

we have observed it to lead to a fragmentation of the solitary wave into the staggered structures, a feature which would not be "accessible" in the continuum limit. It should also be pointed out that despite our computation for different domain sizes as a function of $\Lambda$ for large (approaching the continuum) values of $\epsilon$, the concavity of the relevant eigenvalue dependence precludes a straightforward determination of the associated critical value of $\Lambda$. It can be safely inferred that the instability (at least for sub-critical exponents $k < 2/n$ for $n$-dimensional generalizations of the model) is absent in the nonrelativistic Schrödinger limit. However, further systematic computations of the instability in the $(k, \Lambda)$ plane in the continuum limit are certainly of interest.

Naturally, the present investigation, as a primary one of its kind, raises a considerable volume of additional questions meriting future examination both at the discrete and at the continuum limit. In particular, a key issue is how the discrete model asymptotes to the actual corresponding continuum. It is especially important to understand how the spectral properties may be modified in the limit. Another very interesting avenue of research would be to develop and utilize the solvability conditions that were especially handy in the DNLS case to understand the unusual existence and stability features in the corresponding Dirac case. Understanding also better the role (especially in the dynamics) of the unusual staggered structure would be especially relevant. Other themes, such as a classification of the dynamical instability scenaria for different states or the identification of the exponential instability in the near-linear limit of small $k$ have also emerged. Beyond the realm of "single pulses" focused upon herein, the cases of multi-pulses, pulse interactions and related themes are entirely open, to the best of our knowledge, not only in the discrete case but largely also in the continuum one. Finally, all these investigations could naturally be generalized to higher dimensions, where also vortical and related structures could potentially arise [5, 6]. Some of these topics are currently under investigation and will be reported in future publications.

**Acknowledgements**

This work was supported in part by the U.S. Department of Energy (A.S.). P.G.K. acknowledges support from the National Science Foundation under grants CMMI-1000337, DMS-1312856, from FP7-People under grant IRSES-606096 from the Binational (US-Israel) Science Foundation through grant 2010239, and from the US-AFOSR under grant FA9550-12-10332. We are indebted to Faustino Palmero for technical assistance with some parts of the manuscript.

---

[1] P.G. Kevrekidis, D.J. Frantzeskakis, and R. Carretero-González, *Emergent Nonlinear Phenomena in Bose-Einstein Condensates*, Springer-Verlag, Berlin, 2008.
[2] Yu.S. Kivshar and G.P. Agrawal, *Optical solitons: from fibers to photonic crystals*, Academic Press (San Diego, 2003).
[3] C. Sulem and P.L. Sulem, *The Nonlinear Schrödinger Equation*, Springer-Verlag (New York, 1999).
[4] M.J. Ablowitz, B. Prinari and A.D. Trubatch, *Discrete and Continuous Nonlinear Schrödinger Systems*, Cambridge University Press (Cambridge, 2004).
[5] P. G. Kevrekidis, *The Discrete Nonlinear Schrödinger Equation: Mathematical Analysis, Numerical Computations and Physical Perspectives*, Springer-Verlag (Heidelberg, 2009).
[6] D.E. Pelinovsky, *Localization in Periodic Potentials: From Schrödinger Operators to the Gross-Pitaevskii Equation*, Cambridge University Press (Cambridge, 2011).
[7] S.Y. Lee, T. K. Kuo, and A Gavrielides, Phys. Rev. D **12**, 2249 (1975).
[8] F.M. Toyama, Y. Hosono, B. Ilyas, Y. Nogami, J. Phys. A **27**, 3139 (1994).
[9] D. J. Gross and A. Neveu, Phys. Rev. D **10**, 3235 (1974).
[10] W. Thirring, Annals Phys. **3**, 91 (1958).
[11] N. Boussaïd and A. Comech. *On spectral stability of the nonlinear Dirac equation*. Preprint. ArXiv:1211.3336 [math.AP].
[12] N. Boussaïd, S. Cuccagna, Comm. PDE **37**, 1001 (2012).
[13] D.E. Pelinovsky and Y. Shimabukuro, Lett. Math. Phys. **104** (2014) 21.
[14] A. Contreras, D.E. Pelinovsky and Y. Shimabukuro. ArXiv:1312.1019 [math.AP].
[15] D.E. Pelinovsky and A. Stefanov, J. Math. Phys. **53**, 073705 (2012).
[16] A. Comech, M. Guan, S. Gustafson, Annal. Inst. Henri Poincaré (C) **31**, 639 (2014).
[17] A. Comech, G. Berkolaiko, A. Sukhtayev, arXiv:1306.5150.
[18] F. Cooper, A. Khare, B. Mihaila and A. Saxena. Phys. Rev. E **82**, 036604 (2010).
[19] S. Shao, N.R. Quintero, F.G. Mertens, F. Cooper, A. Khare, A. Saxena, Phys. Rev. E **90**, 032915 (2014).
[20] F.G. Mertens, N.R. Quintero, F. Cooper, A. Khare and A. Saxena. Phys. Rev. E **86**, 046602 (2012).
[21] J. Dalibard, F. Gerbier, G. Juzeliünas, and P. Öhberg, Rev. Mod. Phys. **83**, 1523 (2011).
[22] Y.-J. Lin, R. L. Compton, K. Jiménez-García, J. V. Porto, and I. B. Spielman, Nature **462**, 628 (2009).
[23] Y.-J. Lin, K. Jiménez-García, and I. B. Spielman, Nature, **471**, 83 (2011).
[24] C. Qu, C. Hamner, M. Gong, C. Zhang, and P. Engels, Phys. Rev. A **88**, 021604(R) (2013);
[25] L.J. LeBlanc, M. C. Beeler, K Jiménez-García, A. R. Perry, S. Sugawa, R.A. Williams and I. B. Spielman, New J. Phys. **15**, 073011 (2013).

[26] Jin-Yi Zhang, Si-Cong Ji, Zhu Chen, Long Zhang, Zhi-Dong Du, Bo Yan, Ge-Sheng Pan, Bo Zhao, You-Jin Deng, Hui Zhai, Shuai Chen, and Jian-Wei Pan Phys. Rev. Lett. **109**, 115301 (2012).
[27] X.-Q. Xu and J. H. Han, Phys. Rev. Lett. **107**, 200401 (2011).
[28] J. Radić, T. A. Sedrakyan, I. B. Spielman, and V. Galitski, Phys. Rev. A **84**, 063604 (2011); B. Ramachandhran, B. Opanchuk, X-J. Liu, H Pu, P. D. Drummond, and H. Hu, Phys. Rev. A **85**, 023606 (2012).
[29] T. Kawakami, T. Mizushima, M. Nitta, and K. Machida, Phys. Rev. Lett. **109**, 015301 (2012).
[30] G. J. Conduit, Phys. Rev. A **86**, 021605(R) (2012).
[31] O. Fialko J. Brand, and U. Zülicke, Phys. Rev. A **85**, 051605(R) (2012) .
[32] V. Achilleos, J. Stockhofe, P. G. Kevrekidis, D. J. Frantzeskakis, and P. Schmelcher, EPL **103**, 20002 (2013)
[33] M. Merkl, A. Jacob, F. E. Zimmer, P. Öhberg, and L. Santos, Phys. Rev. Lett. **104**, 073603 (2010).
[34] V. Achilleos, D. J. Frantzeskakis, P. G. Kevrekidis, and D. E. Pelinovsky, Phys. Rev. Lett. **110**, 264101 (2013).
[35] Y. Xu, Y. Zhang and B. Wu, Phys. Rev. A **87**, 013614 (2013).
[36] Y. V. Kartashov, V. V. Konotop, and F. Kh. Abdullaev, Phys. Rev. Lett. **111**, 060402 (2013).
[37] H. Sakaguchi, B. Li and B.A. Malomed, Phys. Rev. E **89**, 032920 (2014).
[38] P.G. Kevrekidis, B.A. Malomed and Z. Musslimani, Eur. Phys. J. D **23**, 412 (2003).
[39] R.S. MacKay and S. Aubry, Nonlinearity **7** (1994) 1623-1643.
[40] C. Hamner, Y. Zhang, M.A. Khamehchi, M.J. Davis, P. Engels, arXiv:1405.4048.
[41] G.L. Alfimov, P.G. Kevrekidis, V.V. Konotop and M. Salerno, Phys. Rev. E **66**, 046608 (2002).
[42] L. Hadzievski, A. Maluckov, M. Stepić and D. Kip, Phys. Rev. Lett. **93**, 033901 (2004).
[43] T. R. O. Melvin, A. R. Champneys, P. G. Kevrekidis, and J. Cuevas, Phys. Rev. Lett. **97**, 124101 (2006).
[44] S. Aubry, Physica D **216** (2006) 1.
[45] M. Johansson and Yu.S. Kivshar. Phys. Rev. Lett. **82** (1999) 85.
[46] R. Carretero-González, J.D. Talley, C. Chong and B.A. Malomed. Physica D **216** 77 (2006).
[47] see e.g. R.A. Vicencio and M. Johansson, Phys. Rev. E **73**, 046602 (2006) and references therein.
[48] G. Berkolaiko and A. Comech. Math. Model Nat. Phenom. **7** (2012) 13.
[49] A. Comech. *On the meaning of the Vakhitov-Kolokolov stability criterion for the nonlinear Dirac equation*. Preprint. ArXiv:1107.1762v2 [math.AP].
[50] A. Comech. *Linear instability of nonlinear Dirac equation in 1D with higher order nonlinearity*. Preprint. ArXiv:1203.3859v2 [math.AP].
[51] J. Xu, S. Shao and H. Tang, J. Comp. Phys. **245** (2013) 131.
[52] D. Pelinovsky and Y. Shimabukuro, *Transverse instability of line solitons in massive Dirac equations*, preprint (2014).
[53] G. James, P.G. Kevrekidis and J. Cuevas, Physica D **251**, 39 (2013).
[54] F. Lederer, G.I. Stegeman, D.N. Christodoulides, G. Assanto, M. Segev and Y. Silberberg, Phys. Rep. **463**, 1 (2008).